

3.0 EXPERIMENTAL

3.1 Printing Experiments

3.1.1 IGT Testing

The IGT Printability Tester AIC2-5 Series 414.Z at the National Printing Laboratory, Department of Chemical Engineering, Monash University was chosen for the laboratory printing experiments as it is used as a preliminary indicator of linting at Norske Skog, Tasman Mill, NZ.

Details of the procedure used at Norske Skog Tasman Mill and the National Printing Laboratory may be found in Appendices A and B respectively.

Two papers of known linting propensity, one high and one low, were sourced from Norske Skog, Tasman Mill to establish the set of variables on the IGT Printability Tester which duplicated the known linting propensity of the paper samples.

The following variables were changed in order to establish the correct settings for the IGT Printability Tester.

Variable	Range Tested	Units
Ink Volume	0.1 – 0.35	ml
Ink Film Thickness	2 – 8	µm
Constant / Acceleration mode	Constant and Acceleration modes	
Printing Speed	1 – 7	ms ⁻¹
Printing Nip Pressure	625 – 800	N
Ink	IGT Picking Test Ink, normal tack, 408002 IGT Picking Test Ink, high tack, 408003	

Table 3.1 – Variable ranges considered in setup of IGT Printability Tester

Appendix C shows the experimental matrix considered while developing the settings for the IGT experiments. The ink volume of 0.7 ml, previously used for hand sheet experiments by R. Koehly [10] was inappropriate and excessive for the machine made paper. This is due to the lower surface roughness of the machine made paper compared with the hand sheets. An ink volume that gave sufficient print density and covered the test sample in sufficient ink was chosen.

The constant speed setting allowed for a larger region of analysis and was chosen as the preferred setting. Limited linting / picking was achieved at lower print speeds, so a print speed was chosen where linting was definitely occurring on the high linting sample and hardly occurring on the low linting sample

The experiment was not overly sensitive to printing pressure, so an upper pressure setting was chosen to ensure sufficient pressure in the nip to give adequate ink coverage.

Experiments in ink tack showed a significant increase in linting / picking when the high tack ink was used. However, the high tack ink was unable to distinguish between the high linting paper and the low linting paper under most conditions. For this reason, the normal tack ink given in Table 3.1 was used.

After a series of experiments, it was concluded by visual analysis that the following set of variables was most appropriate for determining the linting propensity of newsprint. This is the set of variables that showed considerable linting on the high lint paper and low linting on the low lint paper.

Variable	Setting	Unit
Ink Volume	0.2	ml
Ink Film Thickness	5	μm
Constant / Acceleration mode	Constant speed mode	
Printing Speed	4	ms^{-1}
Printing Nip Pressure	800	N
Ink	IGT Picking Test Ink, normal tack, 408002	
Printing Disc	50mm wide, covered with coated rubber 80 Shore A	

Table 3.2 – Variables for setup of IGT Printability Tester

Table 3.3 shows the variables used by Norske Skog Tasman Mill. Appendix A has the full set of procedures for the test conducted at Norske Skog Tasman Mill.

Variable	Setting	Unit
Ink Volume	0.15	ml
Ink Film Thickness	3.6	μm
Constant / Acceleration mode	Constant speed mode	
Printing Speed	2.5	ms^{-1}
Printing Nip Pressure	625	N
Ink	Sicpa stable high tack ink (11056096)	
Printing Disc	50mm wide, covered with coated rubber 80 Shore A	

Table 3.3 – Variables for setup of IGT Printability Tester at Norske Skog Tasman Mill

Although pick tests are usually conducted under accelerated speeds, this series was conducted at constant speed, which is supported by literature. [7] Norske Skog Tasman Mill also conducts the test under constant speed.

The printing speed, printing pressure and ink volume vary slightly between the experiments conducted and the procedure at Norske Skog, Tasman Mill because the ink differed between the two. The experimental test conditions used for the work in this theses were selected to

replicate the results of the Norske Skog test by producing high lint on the high lint sample and barely any lint on the low lint sample.

Six unique samples of newsprint branded Image / Norstar from Norske Skog, Boyer Mill were tested on the top side and bottom side with 3 replicates for each sample. These samples were submitted for analysis by Norske Skog, Boyer Mill based on interesting results that had been obtained from their own internal mill quality and audit testing.

Sample Number	Boyer Roll Number Reference
B1	B0069368
B2	B0074346
B3	B0067718
B4	B0076485
B5	B0076570
B6	B0069624

Table 3.4 – Paper sample references

When the Printing disc has been inked and printed, there is residual ink on the printing disc. The IGT Printability Tester manual indicates that a calculation can be made to determine the amount of ink which has been removed and then this amount can be added to the inked up printing disc to start a new experiment. This approach was tried but found to be unsuccessful as the results obtained did not correlate well with those obtained from freshly cleaned printing discs. Due to this, the author advises that clean, uninked printing discs be used for each print run on the IGT Printability Tester.

In addition to performing the printing experiments, the paper samples were weighed before and after printing to determine the amount of ink applied to the surface of the sheet. This was calculated as 2.4 gm^{-2} (Appendix D), for the conditions described in Table 3.2. The ink

applied to each sample was consistent, with a standard deviation of 0.1 gm^{-2} . An alternative method of calculating the ink applied, would be to weigh the inked printing disc before and after printing.

All experiments were conducted in the constant printing speed mode. It was noticed in the printed IGT paper samples that there was a degree of acceleration, even in this mode of operation as the amount of lint removed on the sample increased from start to end of printing. This was apparent in all samples. This is clearly seen in Figure 3.1



Figure 3.1 – More lint removed in latter part of IGT Printed samples, despite constant printing speed

Care must be taken that printed sheets are dry before further analysis is performed.

The time taken to set up equipment and samples for testing of 4 samples is 45 minutes. This includes the time taken to clean the inking equipment prior to testing of subsequent samples.

3.1.2 Quantification of Lint Removed

3.1.2.1 Image Analysis of Printed Paper

The 36 samples of paper (6 samples x 3 replicates for top and bottom) were analysed for area of lint removed by image analysis

The first series of experiments used an optical microscope with a 50 X magnification and camera to capture images of the surface of the paper. This method proved inappropriate due to the surface roughness of the paper and non-homogeneous ink coverage on the paper at this micro level.

At this magnification, it is difficult to distinguish between linting of fine / filler material and the effects of incomplete surface coverage. This can be seen in Figures 3.2 and 3.3 in the regions labeled 1 and 4. Regions labeled 2 and 3 are clearly that of fibre lint. The scale markers represent 500 μm .

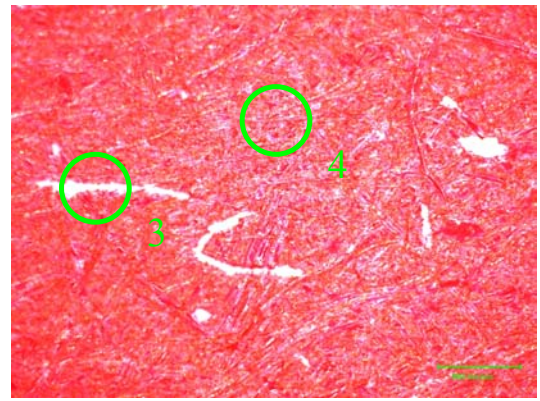
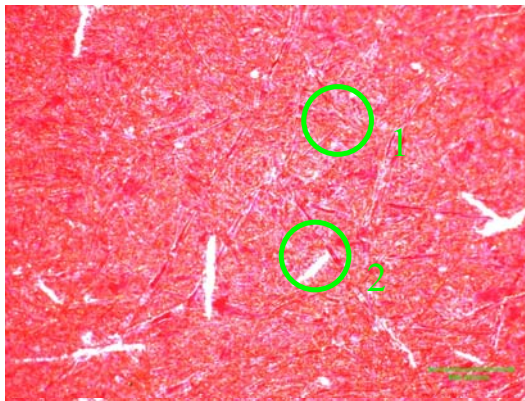


Figure 3.2–Image of IGT Printed Paper–50X Figure 3.3–Image of IGT Printed Paper–50X

An alternative method of capturing the images of IGT Printed paper was sought. A Hewlett Packard Scanjet 6300C Flatbed scanner was used to capture the images. A 1: 1 image was captured (sized 4.8 x 10 cm) at the bottom of the printed image as this represented the area of most lint removal. This is shown in Figure 3.4

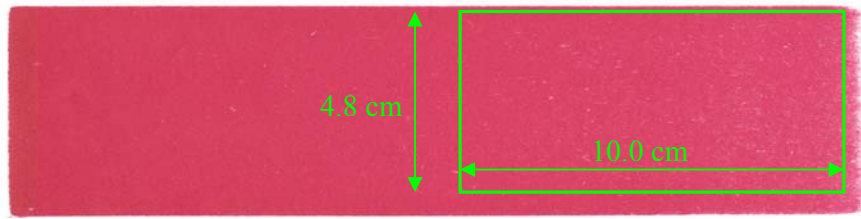


Figure 3.4 – Image captured of printed IGT sample

The images were then analysed by image analysis software, Image Pro Plus, to determine the size distribution of non- printed areas. Figure 3.5 shows the original image. Figure 3.6 shows the areas that have been darkened and then counted as lint by the image analysis software.



Figure 3.5 IGT Test Print 1:1



Figure 3.6 Image analysis quantification

The settings used were Hue : maximum (255), Saturation (94), Intensity : maximum (255)

The particles were counted in three separate bins and then averaged for each duplicate. The full data is reported in Appendix E.

Fines / Filler	0 – 0.05 mm ⁻²
Small Fibres	0.05 – 0.1 mm ⁻²
Fibres	0.1 - 10 mm ⁻²

This method proved to be more representative of the lint that was visually seen on the IGT test prints. This method also allows for a larger area of sample to be considered which is preferred.

3.1.2.2 Image Analysis of Lint

Experiments were conducted to view the type of lint that had been removed from the paper surface during the IGT Printing experiments.

Prior to printing, the printing discs were thoroughly cleaned in a beaker of heptane, in an ultrasonic cleaner for 10 minutes. This ensured that any debris (fibrous, filler or from the cotton rags used to clean the discs) was not present.

After each test print on the IGT printability tester, the printing disc was immersed in a fresh solution of heptane and placed in an ultrasonic cleaner for 10 minutes. This removed the accumulated lint debris from the printing disc.

A methyl violet dye was added to the heptane solution to stain the lint particles. The entire solution was then passed through a vacuum assisted filtration process to separate the carrier solution from the lint particles. Several passes were conducted through the filter (5 µm) to ensure that all lint particles had been collected.

The filtrate was discarded and the lint remaining on the filter paper was analysed under optical microscope as shown in Figures 3.7, 3.8, 3.9 and 3.10.

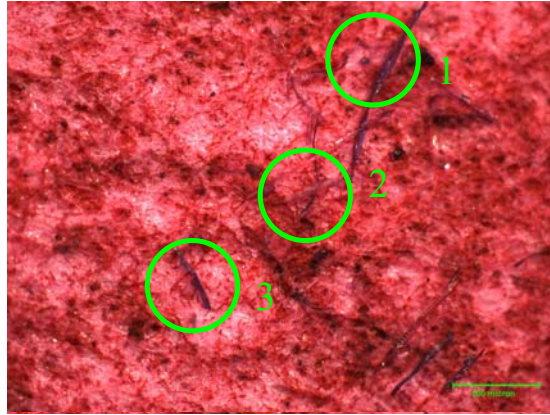


Figure 3.7 – 50 X View of lint debris. The scale marker represents 500 μm .

Regions 1 and 3 in Figure 3.7 clearly show the dyed fibrous lint particles. Closer inspection of the image reveals that some fibrous lint particles, such as that shown lying horizontally in Region 2, are not dyed. The red region in the background is the test ink that has been washed from the IGT printing disc.

Whilst it would be straightforward to conduct image analysis on the filtered lint sample, the results would not be accurate unless all lint particles (fibrous and filler) were stained with the dye, so as to differentiate the lint from the filter medium and ink in solution.

Various methods were used to try and achieve this such as adding the dye at the end of the filtration process, directly onto the filter media, but the same problem persisted.

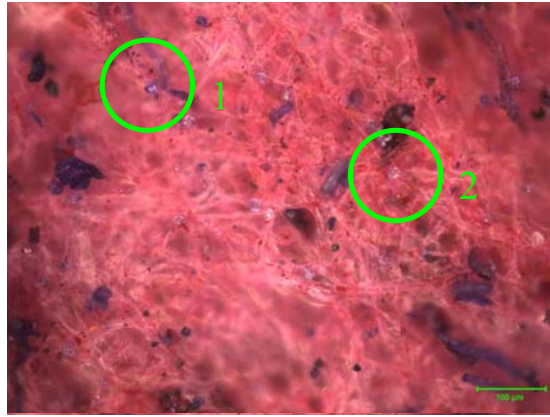


Figure 3.8 - 200X View of lint debris. The scale marker represents 100 μm.

Under a higher magnification it can be seen that non-homogeneous dyeing of lint material is also occurring. Region 1 in Figure 3.8 clearly shows a particle that has been dyed. Region 2 in Figure 3.8 clearly shows a very similar looking particle that has not been dyed. Any visual analysis conducted on such a sample would not be accurate.



Figure 3.9 – 50 X View of lint particles, including a cotton fibre. The scale marker represents 500 μm.

Figure 3.9 clearly shows a cotton fibre in the image. The origin of this cotton fibre is most likely from the rags used to clean the IGT Printability test equipment. It is important to ensure that adequate cleaning of the printing disc takes place prior to any experimentation.

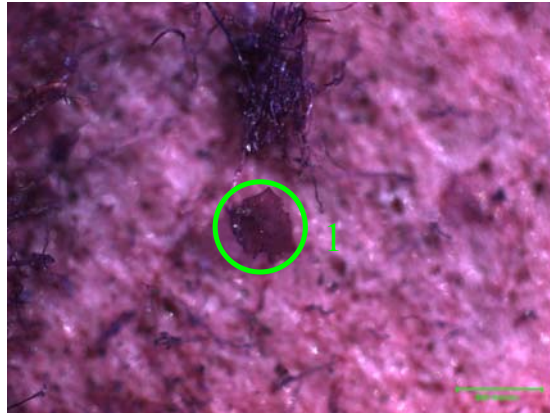


Figure 3.10 – 100 X view of lint particles, including residual ink. The scale marker represents 500 μm .

Region 1 in Figure 3.10 clearly shows a particle of unknown origin that was later identified by FTIR (Norske Skog, Boyer Research Centre) as a piece of ink. In order for image analysis to be conducted accurately on any samples of collected lint, it is important to identify all sources of contamination and remove them.

A clearer differentiation between background ink and dyed lint particles would be obtained if the printing ink was replaced with a clear IGT picking test oil. This would not have replicated the method of lint testing used in this experiment set, as ink was used exclusively to cause linting on the test strips .

In addition, a method was never found to be able to dye all of the lint particles adequately, so as to differentiate from the background filter medium. For these reasons, this technique is not

recommended for the characterization of lint particles and is not used in the results presented in this thesis.

3.1.3 Heidelberg Print Tests

Norske Skog (Boyer Mill) conducts audit testing and quality testing on newsprint by way of a Heidelberg Lint Test.[14] Heidelberg lint is quoted as the amount of lint (gm^{-2}) deposited on an offset press blanket, on a 50 % screen area, after a print run of 7,000 sheets on a Heidelberg GTO52 offset press.[20] It has been noted in literature [1],[2] that the highest lint accumulation is usually in the halftone areas.

The quantity of lint is assessed by weighing adhesive tape strips that are adhered to the blanket and then removed, picking up the deposited lint. [13] Any value greater than 5 gm^{-2} is considered as high, $3 - 5 \text{ gm}^{-2}$ is average and less than 3 gm^{-2} is low. The ink used in this test has a tack of 13 and a densitometer is used throughout the run to ensure that the density of the print is kept close to its target of 0.70 in the full screen area.[13]

The test pattern for the Heidelberg lint test is shown in Appendix F.

Of particular interest is a phenomenon noted by Norske Skog, Boyer Mill. In an area of the test pattern depicting trees, lint often accumulates in a region along the top of the tree line as depicted in Figure 3.11.



Figure 3.11 - Detail of Norske Skog Heidelberg Test Print. Full print shown in Appendix E.

At times the accumulation of lint across the top of the tree line is broad and at other times it is a narrow band of lint accumulation. Microscopic analysis by Norske Skog Boyer has concluded that when the band of lint is broad, the lint is mainly fibrous. When the band of lint is narrow, the lint is mainly filler.

3.2 Filler Size Distribution

Several techniques were trialled to quantify filler size distribution and area in paper surfaces. The development of these techniques is described in this section. During the time available it was not possible to obtain quantitative information for all techniques. However all trials have been included so as to give a starting point for future work.

3.2.1 SEM Backscatter

The aim of the SEM / backscatter experiments were to :

- obtain images of the paper surfaces, top and bottom
- analyse the images to quantify particle size distribution of the filler in the paper surface.

3.2.1.1 Sample Preparation

The paper samples listed in Table 3.4 were cut with a razor knife to 1 cm x 1cm square.

These paper samples were mounted on stubs with double sided adhesive tape.

A small amount of carbon was applied with a brush to the corner of the sample to earth the sample to the stub. The sample was then coated with carbon in a Dynavac CS300 sputter coater with an aim coating thickness of 240 angstroms. This final coating is to make the sample electrically conductive.

The samples were then ready for use in the microscope.

3.2.1.2 Microscopic Analysis

A Phillips XL30 Field Emission Scanning Electron Microscope, located at CSIRO, Forestry and Forest Products, Clayton, Vic. was used for the microscopic analysis.

The stubs were mounted securely onto a carousel, which in this case carried six unique samples. Air was evacuated from the chamber and the microscope set up with the desired variables to view the samples.

The SEM produces electrons that impinge on the sample. A variety of signals can be captured due to interaction of the impinging electrons with the sample :

- Secondary electrons
- Backscatter electrons
- X-rays

There are different interaction volumes for each signal, as shown in Figure 3.12.

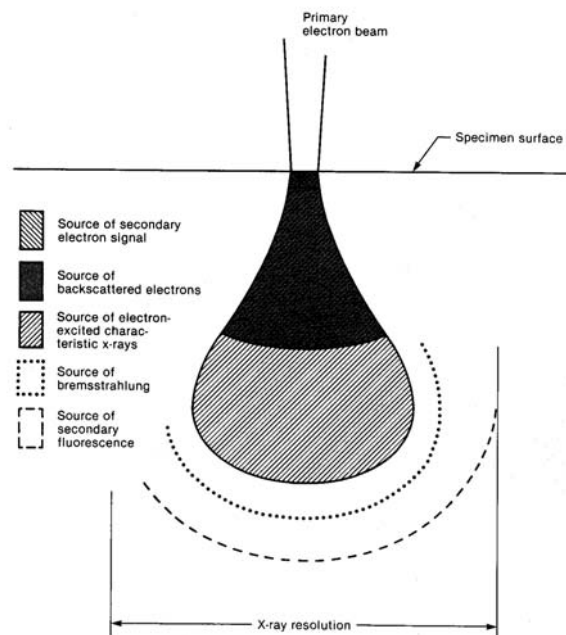


Figure 3.12 Illustration of interaction volumes for electron/sample interactions [21]

The popularity of SEM is partly due to its ease of operation. It is very sensitive to low concentrations, is non destructive and requires minimal sample preparation. [21]

Secondary Electrons

Secondary electrons are the electrons that escape from the sample when the primary electron impinges. [21] Secondary electrons are more commonly known as any secondary electron that is less than 50 eV in energy.[22] These secondary electrons with little energy can only be detected if they are created near the surface of the sample. [21]. For this reason it is very important that the sample is flat on the stub.

The greatest density of secondary electrons is created by the primary beam before it has a chance to spread and therefore the spatial resolution is very high. The topographic sensitivity and high spatial resolution make secondary electron images very popular for micrographic images such as that shown in Figure 3.13.[21] Secondary electron images are not able to differentiate consistently between the filler and fibre particles in a paper sample as they do not carry information on elemental composition of the sample.

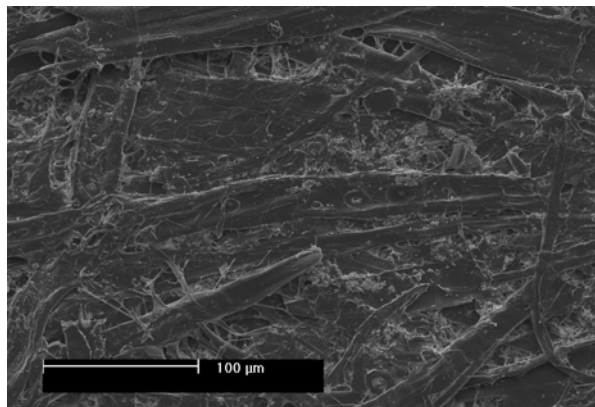


Figure 3.13 - 250X Secondary Electron image of B1 bottom side

Secondary electron images were obtained for each of the 6 samples analysed on the top and bottom surfaces. These images were taken as reference images only. No further analysis was undertaken with these images.

Backscattered electrons

If the primary electron interacts with the nucleus of the sample atom, an electron may scatter in any direction with little loss of energy. This electron is known as a back scattered electron and is much more energetic than a secondary electron. It is generally more than 50 eV in energy. [22] and can come from a greater depth in the sample. Because of the increase in the depth over which backscattered electrons are generated, the backscatter technique will have a lower spatial resolution than can be obtained by measuring secondary electrons.[21]

However, due to the fact that backscattered electrons interact with the nucleus of an atom, they are able to distinguish between differences in atomic number. The higher the atomic number in the sample, the greater the positive charge of its nucleus and the more likely that an electron will produce a backscattered electron. [21]

The clay filler in the paper sample is $\text{Al}_2\text{Si}_2\text{O}_7$. Aluminium and Silicon have an atomic number of 13 and 14 respectively. The carbon in the cellulose has an atomic number of 6. It can be seen in Figure 3.14 that the aluminium and silicon atoms (in the filler) produce a strong backscatter signal, thereby enabling the differentiation between filler and fibre in the paper sample.

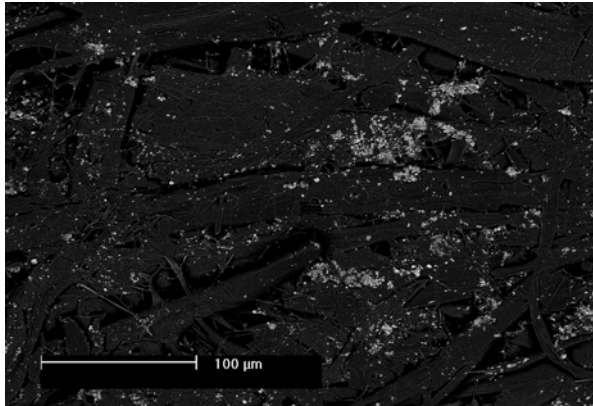


Figure 3.14 - 250X Back Scattered Electron image of B1 bottom side

Back scattered electron images are able to differentiate between elements if the atomic number differs by more than 3.[22] This is why there is such a good differentiation between the filler (Al and Si) and the fibre (C). There is no differentiation between the Al and Si, since they are only one atomic number apart. This is useful for our analysis as it allows the clay particle / agglomerate to be grouped as a whole.

The set up for the SEM in backscatter mode is very sensitive, with numerous variables to be considered before specifying the correct set up for a particular experimental set. Sub-optimal setup of the SEM may result in sub-optimal images for subsequent image analysis. The quality and accuracy of the image obtained is paramount.

Substantial time and effort was therefore committed to this part of the experimental work, to obtain the optimal settings to conduct the experiments under. The following settings were used for the work conducted in back scatter mode.

Variable	Setting
Accelerating Voltage	5 kV
Spot Size	5
Working Distance	10.5 cm
Brightness	34.6 %
Contrast	95.9 %
Magnification	250 %

Table 3.5 – Settings for SEM Experiments

Twenty back scattered electron images were obtained for each of the six paper samples, top and bottom, totaling 240 images in all.

X-Rays

The source (primary) electron ejects an electron from an inner shell of a sample atom. The resulting vacancy is then filled by an electron from a higher-energy shell in the sample atom. In dropping to a state of lower energy, the vacancy filling electron must give up some of its energy. This energy appears in the form of electromagnetic radiation (an x-ray) and is equal to the energy difference between the two electronic levels involved. Each element in a sample, when subjected to the bombardment of electrons will emit a unique and characteristic pattern of x-rays. [21]

X-Rays generated from electron transitions in atoms are particular to an element due to characteristic energies associated with the x-rays. In this way, theoretically x-ray analysis from the SEM could be used to differentiate between the filler (Al and Si) component and fibre (C) component of the paper sample.

X-Rays however, travel much greater distances through the sample than the secondary or backscattered electrons and as a result, the spatial resolution is less.[21]

An illustration of the interaction volumes for electron / sample interactions is given in Figure 3.12 [21]. It shows why x-rays have the poorest resolution, as they come from deepest within the sample.

Experiments were conducted to obtain images of the paper sample by x-ray detection. The resolution was not high enough to show agglomerates of clay known (by back scatter detection) to be within the sample. Images from the x-ray maps were compared to the back-scattered electron images and the resolution of the x-ray map was inferior, displaying small discrete areas of detection of Al and Si, as opposed to the well defined filler vs fibre separation obtained in the back-scattered electron images. Figure 3.15 shows the x-ray detection image, accumulated after 2 hours of scanning. The image is not suitable for image analysis as the filler aggregates can not be seen.



Figure 3.15 – X-Ray Map of surface of paper sample

Further experiments were conducted, capturing data over a longer time frame. The original back scattered image is shown in Figure 3.16. Figure 3.17 shows the image with Aluminium mapped. This is a blurred replica of the image acquired with the back scatter detector.

Figure 3.18 shows the aluminium and the silicon mapped. This image shows improved clarity over Figure 3.17, which shows aluminium only, but it is still inferior to the back scatter image in Figure 3.16. The data acquisition took place over 15 hours and was taken at a magnification of 250 % and 10 keV beam current.

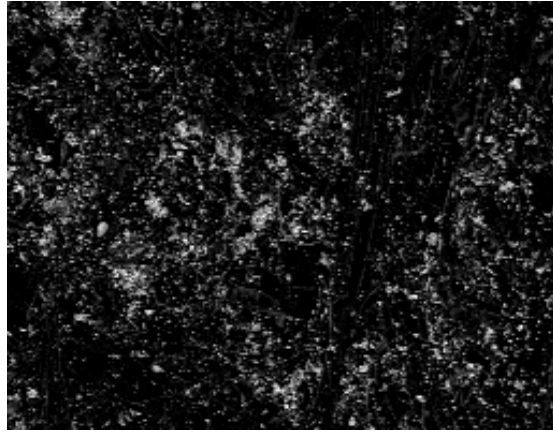


Figure 3.16 – Back Scatter Image of B3 Top

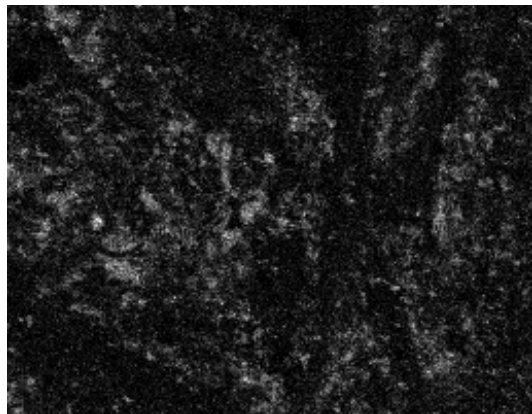


Figure 3.17 – Aluminium X-Ray Map of B3 Top

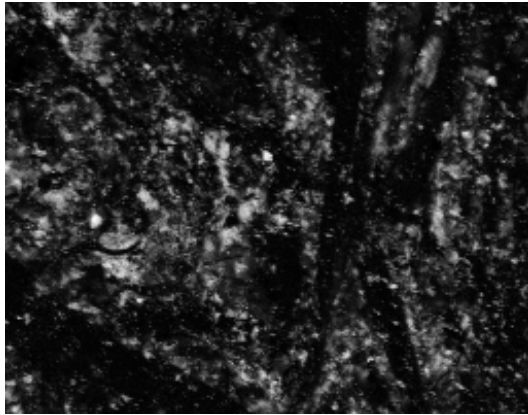


Figure 3.18 – Aluminium and Silicon X-Ray Map of B3 Top

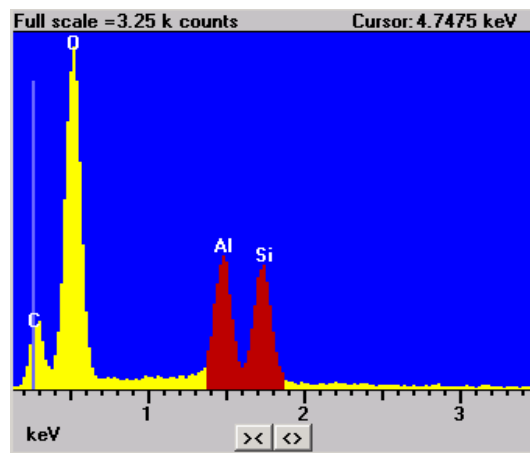


Figure 3.19, Spectrum of x-rays detected in B3, top

Figure 3.19 shows the spectral peaks of Carbon, Oxygen, Aluminium and Silicon, all found in the paper samples. The excitation energies are as follows: Al (1.487 keV), Si (1.74 keV), O (0.525 keV), C (0.277 keV).

Of the three techniques investigated using the SEM, only the back scatter and x-ray can distinguish between filler and fibre. The x-ray technique suffers from poor resolution and the

long time required to capture a single image. Therefore the back scatter technique was chosen for the next step in the experiment – quantification of the filler particle distribution by image analysis.

3.2.1.3 Image Analysis

The twenty back scattered electron images, obtained for each of the six paper samples, top and bottom, totaling 240 images in all, were subjected to image analysis using XL-Pro Image Analysis software at CSIRO, Forestry and Forest Products, Clayton, Vic.

The image was analysed by using a grey level threshold set at 111 out of a maximum of 255, which separated the filler particles adequately from the fibre particles and ensured that fibre particles were not included in the filler count.

An example of a back scattered image is shown in Figure 3.20.

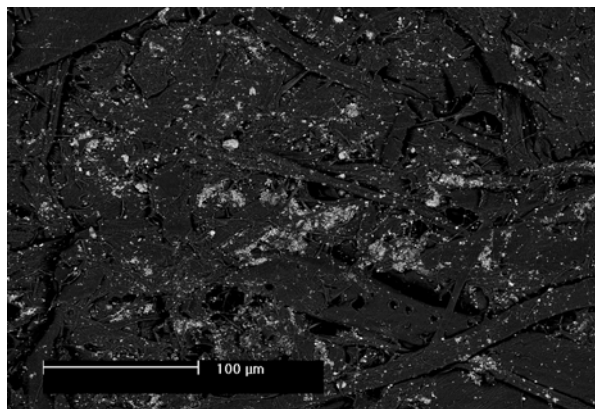


Figure 3.20 – 250X Back Scattered electron image of B2 Top side

The filler particles can then be clearly distinguished from the fibre and may be counted and allocated into nominated bins.

The bins chosen for this study are given in Table 3.6

ID Class	Size (um ²)	Colour
1	0 – 4	Red
2	4 – 8	Green
3	8 – 16	Dark Blue
4	16 – 50	Yellow
5	>50	Light Blue

Table 3.6 – Particle bins for image analysis

Figure 3.21 shows the image shown in Figure 3.20 after thresholding and allocating the particles into different bins according to the surface area size. Each particle that has been counted has then been coloured according to the classification scheme given in Table 3.6.

Classes 1 –3 are nominally very fine particles that may be considered as dust. Classes 4 –5 are more likely to be candidates for linting that may be visually seen in a printed sheet of newsprint.

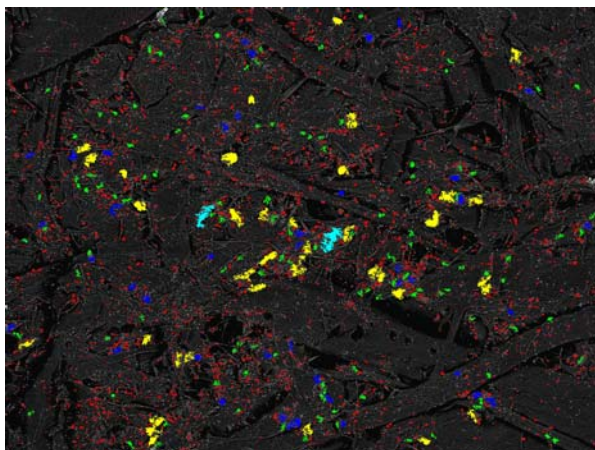


Figure 3.21 – 250X Back Scattered electron image with particles counted and binned of B2 Top side

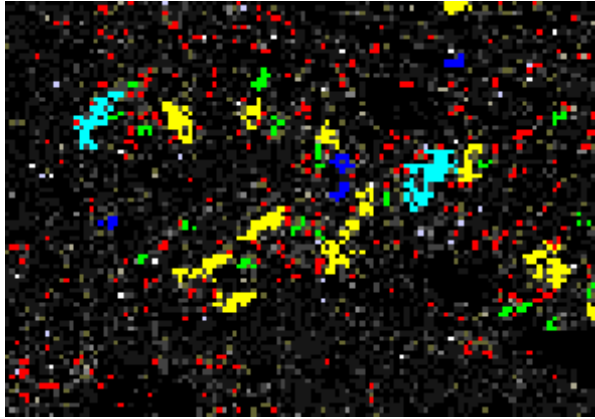


Figure 3.22 – Enlargement of detail of Figure 3.21 to illustrate more clearly relative sizes of the binned particles.

It is of utmost importance to choose the correct SEM settings to capture correct images with the SEM. If sub-optimal variables are set, then the probability of counting non filler particles as filler, or not counting all of the filler particles is increased.

Figures 3.23 and 3.24 show images that have been captured using sub-optimal conditions and subsequently when the filler has been counted with image analysis, fibre areas are counted as filler particles, as circled in Region 1 in Figure 3.24.

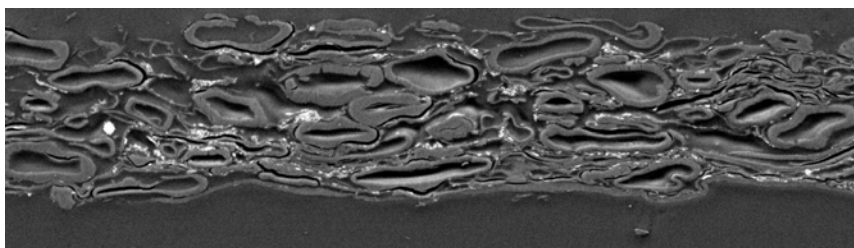


Figure 3.23 – Cross-section of newsprint taken by R. Koehly (2003), [10]

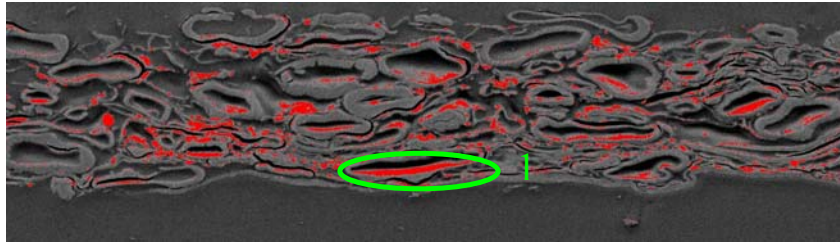


Figure 3.24 – Cross-section of newsprint taken by R. Koehly (2003) , [10] with “filler” particles incorrectly counted.

An improved set of SEM settings in Figures 3.25 and 3.26 shows Region 1, which is “light coloured” in the image, but still not counted as filler, because the thresholds have been correctly set up. The settings used were as given in Table 3.5.

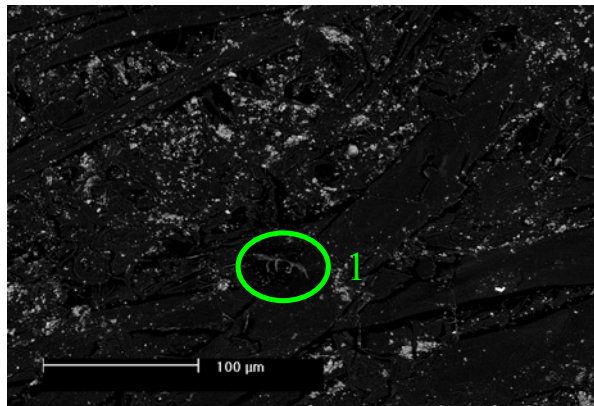


Figure 3.25 250X Back Scattered electron image of B1 Top side

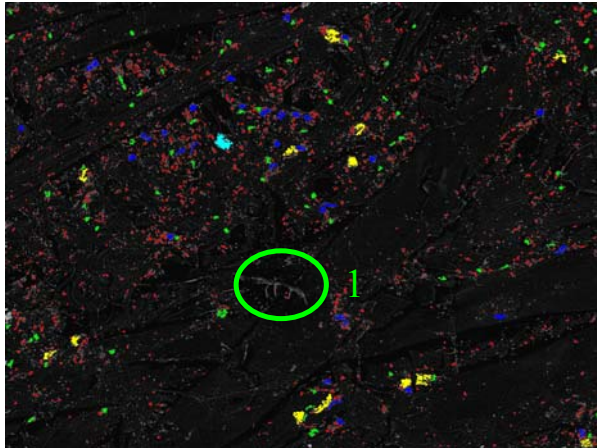


Figure 3.26 - 250X Back Scattered electron image with particles counted and binned of B1
Top side

The software (XL-Pro) has been set up to count and bin particles based on grey levels, This excludes those particles which touch the border of the image as the extension of the particle size beyond the image border is not known. This is shown clearly in Figure 3.27 where a large particle of filler has not been counted because it is adjacent to the border of the image.

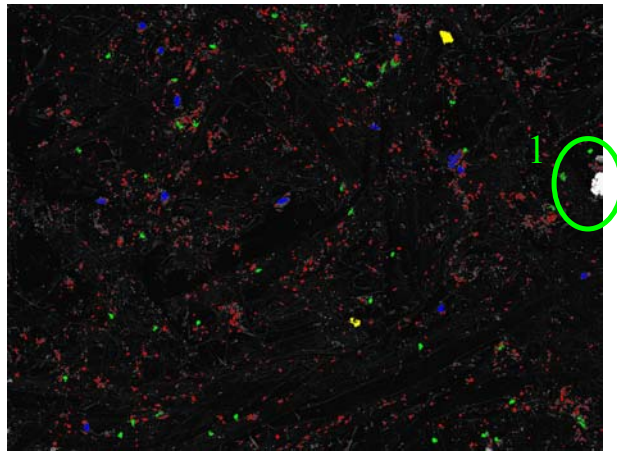


Figure 3.27 - 250X Back Scattered electron image with particles counted and binned of B2
Bottom side

The results for number and area of particles counted for each sample were tabulated and are presented in Appendix G. Each value is the average of twenty individual analyses.

3.2.2 SE Microprobe with X-Ray Detection

As the experiment set using X-Ray mapping with the energy dispersive SEM was unsuccessful as discussed in Section 3.2.1.2, a different approach was attempted. A Jeol scanning electron microprobe with a wavelength dispersive spectrometer located at CSIRO, Department of Minerals, Clayton, Vic. was used for the microscopic analysis.

A microprobe is an electron column designed to deliver stable beam currents of high intensity. These higher beam currents are used to produce sufficient characteristic x-ray intensities, analysed by a wavelength dispersive spectrometer to provide quantitative elemental analysis. [21]

Where the energy dispersive spectrometer (EDS) is useful in obtaining rapid analysis of an unknown sample, the wavelength dispersive spectrometer is preferred for obtaining quantitative information and analysis of light or trace elements.[22] Table 3.7 shows a list of advantages of both systems.

Advantages of Energy Dispersive Spectroscopy

- Compact, low cost
- Rapid
- Simultaneous multi element analysis

- High collection efficiency
- Low sensitivity to geometric effects

Advantages of Wavelength Dispersive Spectroscopy

- Higher resolution
- Higher Count rate
- Highly quantitative
- More distinct peaks
- Higher sensitivity

Table 3.7 Comparison of EDS and WDS [22]

3.2.2.1 Sample Preparation

It was chosen to prepare the samples as thin sections, since the interaction volume of x-rays is very large as shown in Figure 3.12 earlier. Preparing the samples as thin sections reduced the available interaction volume. It was recommended by CSIRO, Department of Minerals, that analysis could not be performed on bulk surface samples.

Paper samples were embedded into an epoxy resin at Monash University, School of Physics and Materials Engineering. This embedding took 4 hours to complete and an additional 2.5 hours to cure at 60⁰C.

The samples were then turned on their sides and thin sections cut from the mould containing the paper sample in the epoxy resin. The thin sections were 120 nm or 0.12 µm deep. The sectioning / cutting was performed with a diamond tipped knife of 0.2 nm in radius in an

ultra-microtome and took 8 hours to complete per sample. This is a highly specialised task and requires a high degree of precision. This work was performed by Sel Glanville from Monash University, School of Physics and Materials Engineering.

The silicates in the paper sample are very abrasive on the knife edge and as such glass knives are not appropriate as they will damage the sample. For this reason, a diamond tipped knife was used.

The samples were then glued to a layer of glassy carbon that is subsequently placed on a stub to be placed inside the SE Microprobe. Figure 3.28 shows a magnified view of the samples on the microscope stub. This was obtained with an optical microscope and camera attachment.



Figure 3.28 – 100X Four cross-sectioned samples of newsprint for SE Microprobe

3.2.2.2 Microscopic Analysis

The prepared samples were analysed using a Jeol Electron Microprobe at CSIRO, Department of Minerals, Clayton, Vic using a 25 kV beam and a beam current of 36 nanoamps. This compares to the low beam current of 5 kV used in the SEM experiments described in Section 3.2.1.2. Each sample was mapped which took 4 – 6 hours per image, depending on the step size and number of pixels. The area imaged is shaded in dark blue on Figure 3.29, as the microprobe energy is high and permanently marks the scanned area.

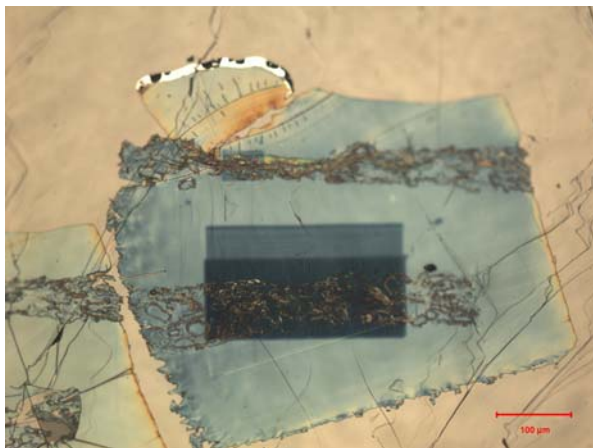


Figure 3.29 – 200X Cross-sectioned sample of B3 newsprint for SE Microprobe

Figures 3.30 and 3.31 show backscatter images taken on Sample B3. Note the rippled effect on the back scatter image due to the creasing of the glassy carbon that has been used as a support in the sample mount. The backscattered images are not as well defined as those shown in Section 3.2.1.2 that were taken by the SEM.

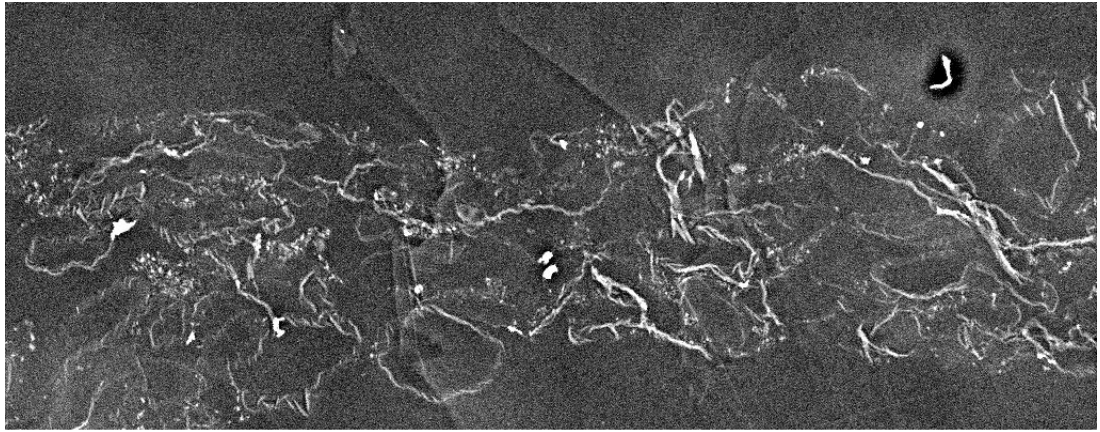


Figure 3.30 – Back scatter image of Sample B3 Cross-section

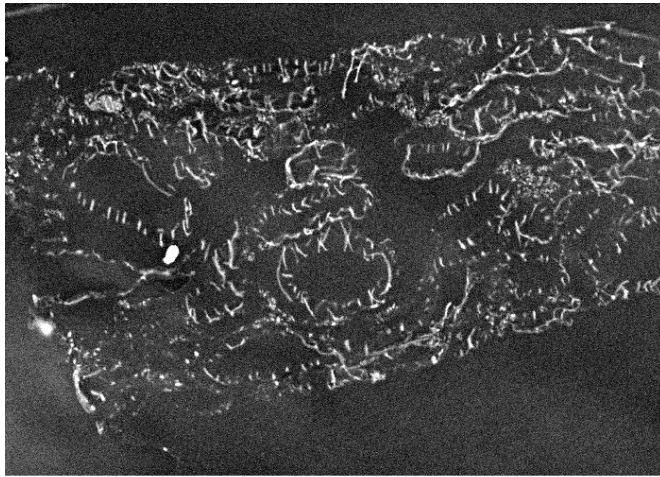


Figure 3.31 – Back scatter image of Sample B3 Cross-section

The X-Rays were detected and produced the following series of images shown in Figures 3.32 – 3.34. Trace elements such as Sodium and Iron were detected in the samples as well as the expected Silicon and Aluminium from the clay filler.

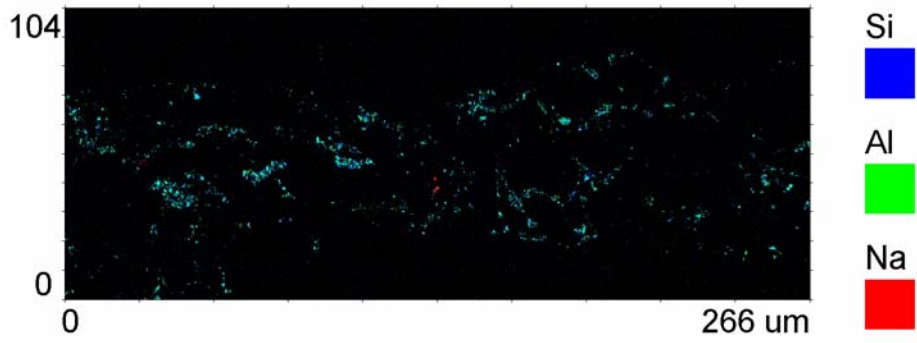


Figure 3.32 – X-Ray Map of Sample B3

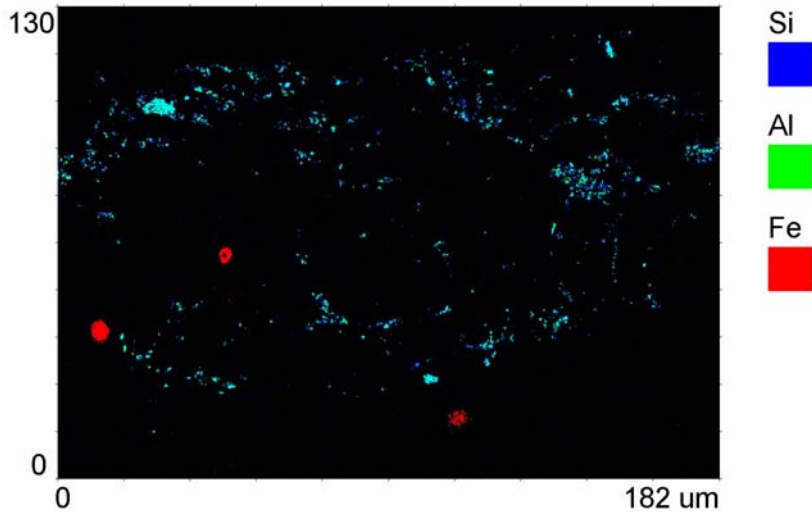


Figure 3.33 – X-Ray Map of Sample B3

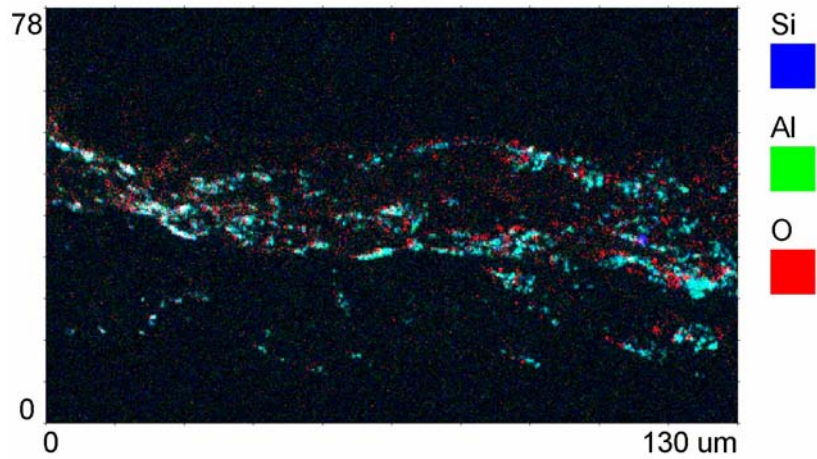


Figure 3.34 – X-Ray Map of Sample B5

Despite the higher resolution of the x-ray images with the aid of the wavelength dispersive spectrometer and the thin sections, the images obtained do not show discrete filler agglomerates. The technique does not pick up all of the elements in all locations. The images obtained can not be used to perform accurate image analysis, to determine particle size distribution.

3.2.3 X-Ray Tomography with Phase Contrast

The X-Ray ultramicroscope is a variation on the SEM principle discussed in Section 3.2.1.2. An X-Ray ultramicroscope located at CSIRO, Manufacturing & Infrastructure Technology, Clayton and operated by X-Ray Technologies (XRT) was used for this set of experiments. The X-Ray ultramicroscope is hosted within a standard SEM. The internal chamber of the SEM with the X-Ray ultramicroscope is shown in Figure 3.35

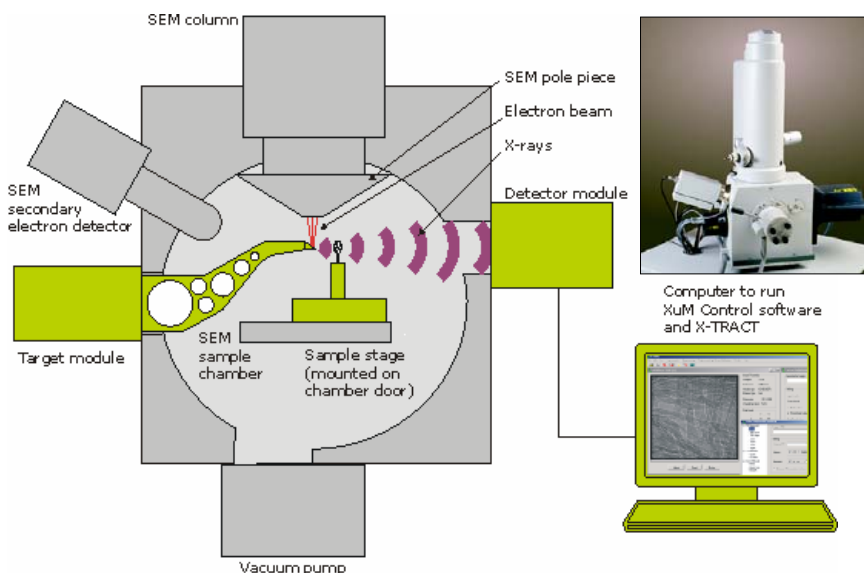


Figure 3.35 - X-Ray ultramicroscope setup. [23]

The electron beam, instead of being directed at the sample, is directed at a platinum target that generates x-Rays of approximately 8 keV. The sample (in this case, measuring 0.5 x 1 mm) is placed upright in a vice, a distance R_1 away from the x-ray source. The x-Rays travel through the sample thickness. Images are projected onto the detector, a distance R_2 away from the sample. Changing the ratio of $R_1 : R_2$ changes the magnification and also the phase contrast. This is shown in Figure 3.36.

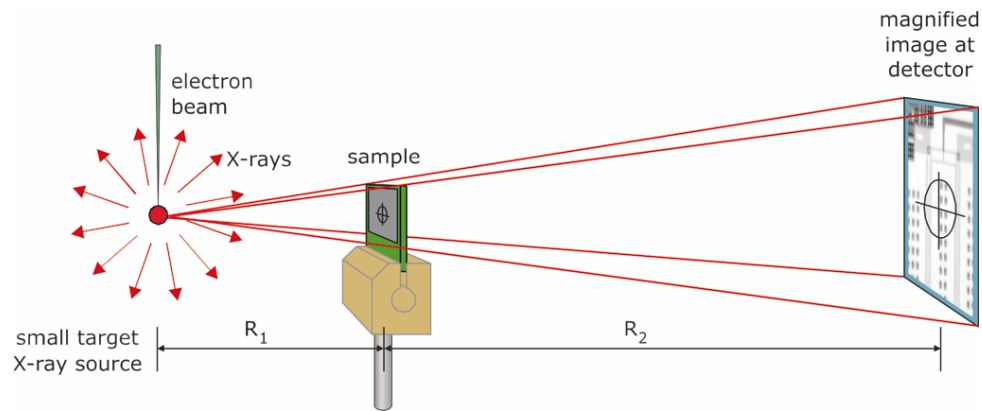


Figure 3.36 – Projection x-Ray Microscopy schematic [24]

Absorption contrast is used to create conventional x-ray images as in medical x-ray imaging. X-rays absorbed by the sample create a shadow at the detector.[24]

Phase contrast is based on the wave properties of x-rays and is a result of the refraction (not absorption) of x-rays. The effects of refracted x-rays are most notable at edges, voids or boundaries of the sample, creating an image of bright and dark fringes at the detector. The projection geometry allows the disturbed wave front to be captured.[24]

X-rays act constructively and destructively in the distance R_2 to produce the image at the detector. The image is a result of x-rays passed through the entire thickness of the stationary

sample and is thus an accumulated effect. Figure 3.37 shows the planar image of a sample of newsprint collected at the detector, spaced R_2 away from the sample. The fibre network can be seen in the image and the areas in Region 1 may be the evidence of filler.

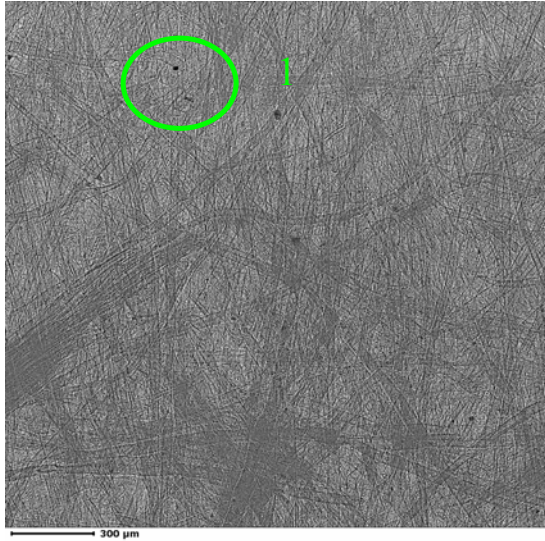


Figure 3.37 – Raw data of planar image, collected at R_2 away from sample [23]

An algorithm is then used to calculate what the image would look like at the object plane (ie $R_2 = 0$). This is shown in Figure 3.38

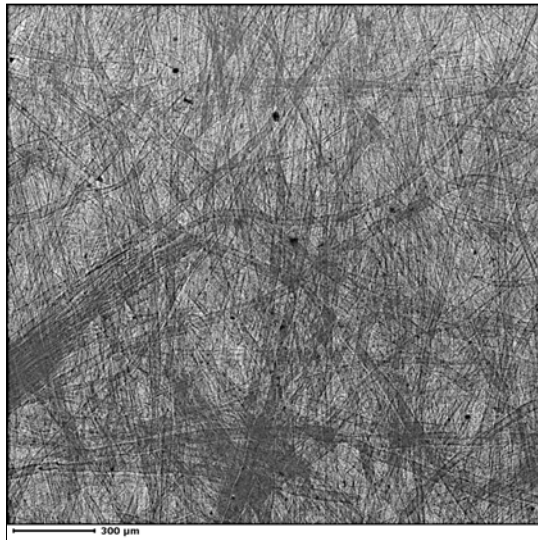


Figure 3.38 – Phase retrieved data of planar image. [23]

In the phase retrieved image, the clarity of the image is improved and further analysis can be conducted to identify particulates and construction of the sample.

Figures 3.39 and 3.40 show an area of interest. This area possibly contains fibres that have lifted out of the surface of the paper. Since the phase contrast relies on refraction, a fibre which has lifted can be seen because the refractive index for a fibre / air interface is different than for a fibre / fibre interface. These lifted fibres could theoretically be used to predict the linting propensity of the paper.

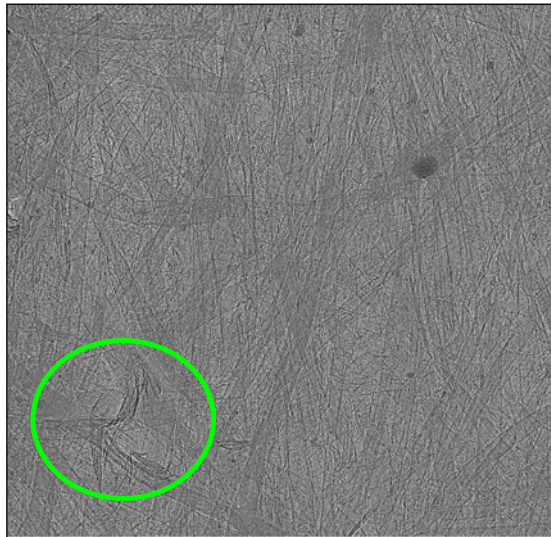


Figure 3.39 Raw Image [23]

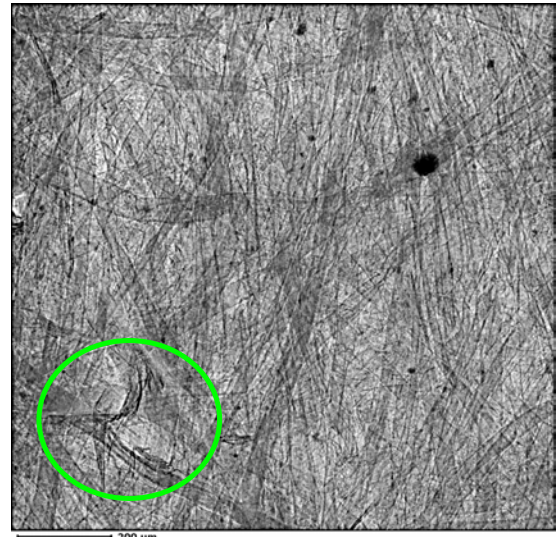


Figure 3.40 Phase retrieved image [23]

This idea is tested further by imaging an area of the paper with a tear in it. The torn area of the paper has fibres that have lifted out of the surface of the paper. Figures 3.41 and 3.42 with the torn area of paper show a similar image to that in 3.39 and 3.40 respectively.

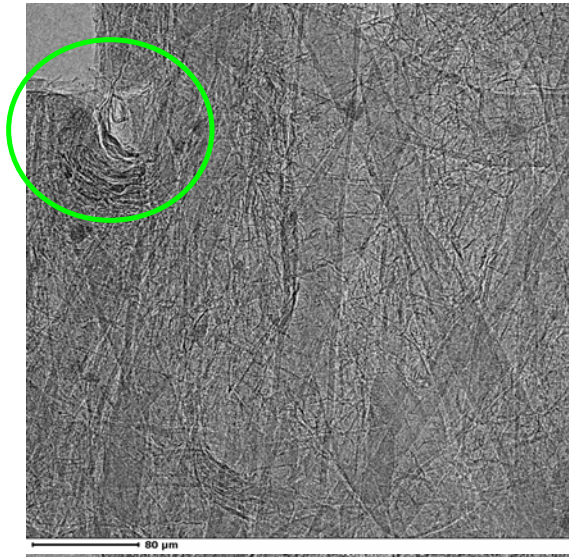


Figure 3.41 Raw Image [23]

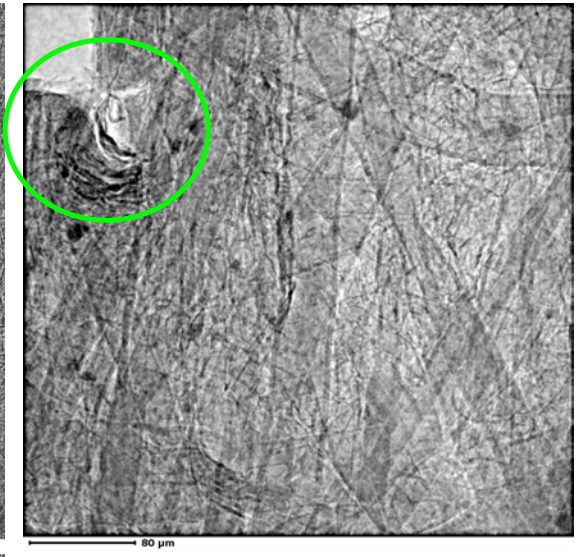


Figure 3.42 Phase retrieved image [23]

If the sample is rotated in the chamber, information can be gathered in sections / layers, enabling an entire 3D model of the sample to be reconstructed. 400 images were acquired for the 3-D reconstruction. Each image took 60 seconds to acquire and this acquisition was automated to run over-night. The 400 images are then used to construct the 3-D reconstruction that takes a further 2 hours to process. A schematic of the process is shown in Figure 3.43

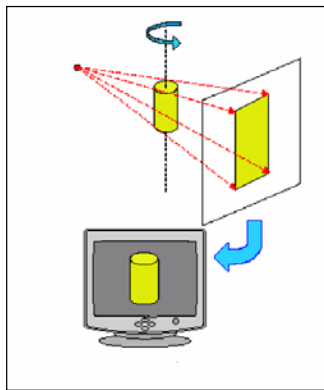


Figure 3.43 – Tomographic Reconstruction [23]

Figures 3.44 – 3.46 show the rotational views of the paper sample as it is being imaged for the 3-D reconstruction

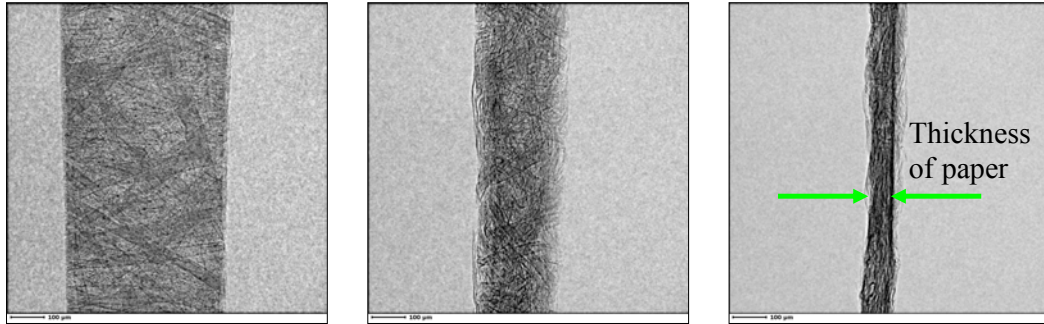


Figure 3.44 Planar View [23] Figure 3.45 Oblique View [23] Figure 3.46 side on view [23]

Figure 3.47 shows the isosurface reconstruction that is constructed by defining the surface boundary of the sample by intensity thresholding. It is constructed from the tomographic reconstruction of the X-Ray data.

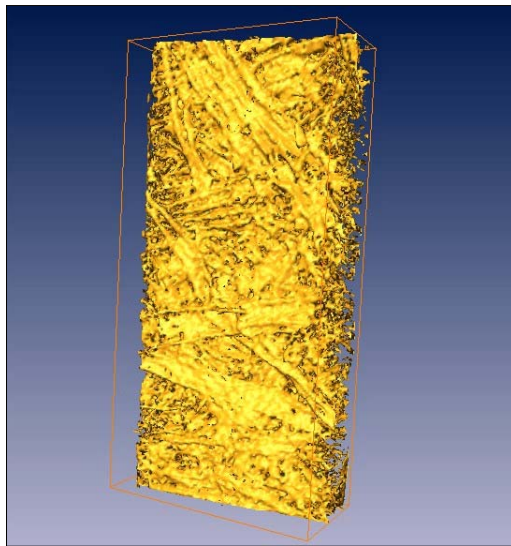


Figure 3.47 – Isosurface reconstruction of paper sample [23]

At this point, slices can be taken at any angle and at any position in the sample. Planar slices have been taken in Figures 3.48 and 3.49. An orthogonal slice has been taken in Figure 3.50.



Figure 3.48 – Virtual planar slice [23]

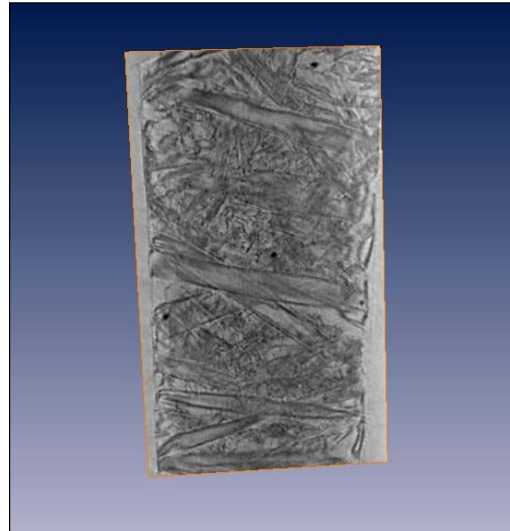


Figure 3.49 – Virtual planar slice [23]

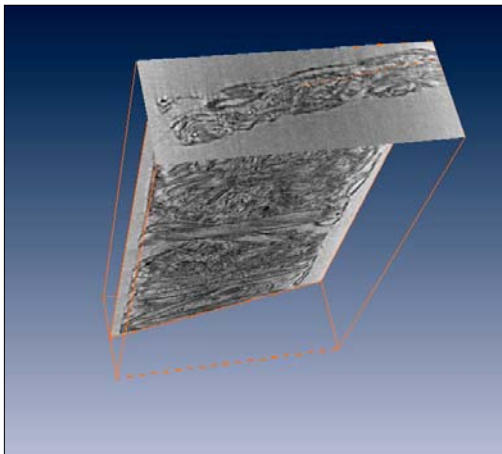


Figure 3.50 – Orthogonal slicing of paper sample [23]

It is possible to select particles based on density and segment them from the rest of the sample. This is the process by which filler particles could possibly be selected and

segmented from the fibre network. Figure 3.51 shows the segmentation of the dark particles that are believed to be filler. Slices could then be taken in any direction in the volume to determine filler distribution.



Figure 3.51 – Particulates in sample volume.[23]

This method has been investigated as a proof of concept at this stage. The author recommends that this method be investigated further to determine the usefulness in determining filler size distributions in paper samples.

Extended work is required in selecting the appropriate intensity thresholds to separate the filler particles from the fibre network. The resolution is $0.3\ \mu\text{m}$ and limited sample preparation is required. This is a non-destructive test method. Sample slices can be taken with thickness of $1\text{-}2\ \mu\text{m}$. The slice thickness is a function of the resolution of the original images that make up the 3-D reconstruction .

3.2.4 FTIR Spectroscopy

Fourier Transform Infrared (FTIR) Spectroscopy is an analytical technique used to identify materials in a sample. A light source is used to produce light in the infrared (IR) region and the sample is subjected to IR light. The sample absorbs different IR light wavelengths according to its chemical properties (molecular components and bonds). A detector is used to collect the radiation that passes through the sample and a mathematical function known as a fourier transform is used to produce a spectrum.

3.2.4.1 Determination of spectra

The Bruker – Equinox 55 FTIR Spectrometer, Department of Chemistry, Monash University was used to obtain spectral data for cellulose and filler.

Two samples of cellulose (fibrous long and microgranular) and one sample of clay filler were analysed. A small amount of sample was placed onto a diamond plate and pressure applied via an anvil to ensure that the sample was flat. The infrared radiation penetrates 2 μm into the sample, measuring the spectra with FTIR in reflectance mode, using a diamond ATR plate. The sample area is 1 mm in diameter.

Figures 3.52 and 3.53 show the spectra obtained for the cellulose fibrous long and cellulose microgranular respectively.

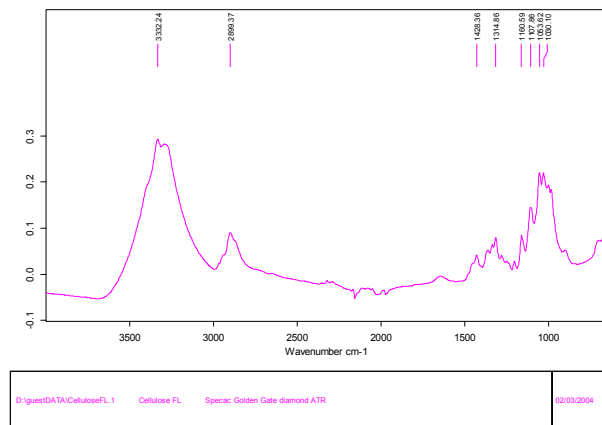


Figure 3.52 – Spectrum of cellulose fibrous long

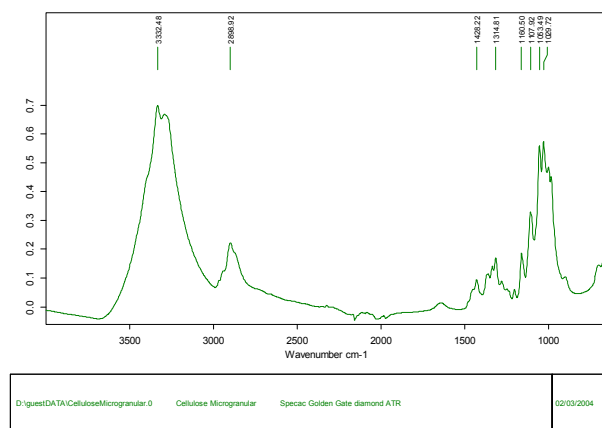


Figure 3.53 – Spectrum of cellulose microgranular

As expected the two spectra for different samples of cellulose are essentially the same. The first peak at 3332 is due to the –OH bond. The second peak at 2899 is due to the –CH₃ and –CH₂CH₃ groups. The large group of peaks from 1428 – 1030 are due to other organic bonds and intra-molecular interactions in the cellulose. These bonds and chemical groups can be seen in Figure 3.54. The chemical formula for cellulose is (C₆H₁₀O₅)ⁿ where n is the degree of polymerisation.[25]

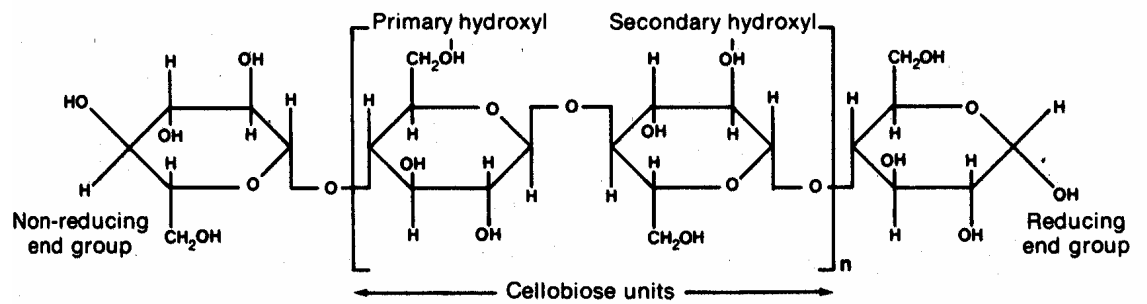


Figure 3.54 – Chemical structure of cellulose [25]

When analyzing a paper structure, other components attached to the cellulose must also be considered, such as lignin, found in newsprint. Figure 3.55 shows the chemical structure of lignin and the associated phenyl propane units.[25] Depending on the pulping used to process the wood fibres, different modifications to the base components would occur, resulting in different spectra.

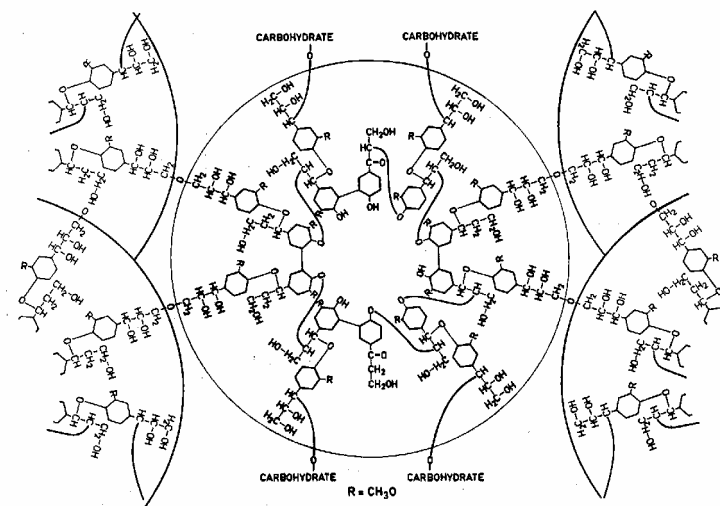


Figure 3.55 – Chemical structure of lignin [25]

The spectra for lignin is shown in Figure 3.56. There are no prominent peaks and will not interfere with the distinction between fibre and filler. The parabolic shape of the curve is due to the white kraft liquor in which the lignin is dissolved. The actual peaks from the lignin are individually marked.

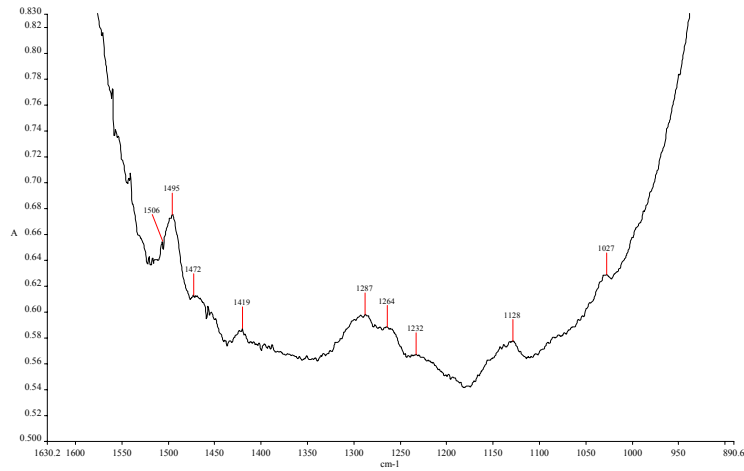


Figure 3.56 – Spectrum for lignin.[26]

The clay was analysed by Bruker FTIR and the spectra is shown in Figure 3.57.

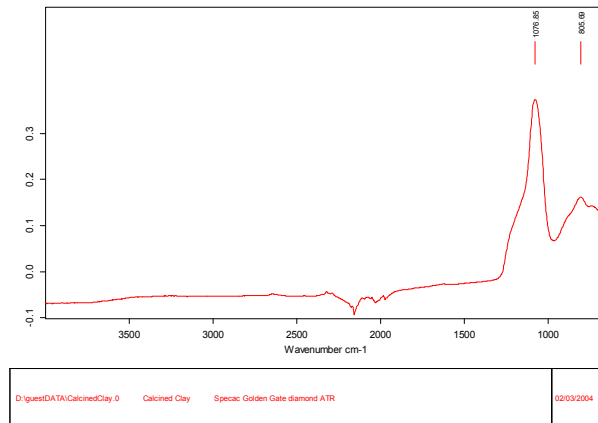


Figure 3.57 – Spectrum for calcined clay

The chemical formula for calcined clay is $\text{Al}_2\text{Si}_2\text{O}_7$. [27] The major peak at 1077 is due to the Al-O and Si-O bonds. These overlap as they emit spectra at similar wave numbers.

The small dip in the spectra around 2200 is due to the diamond plate used in the measurement. This small dip can be found in all of the spectra and should be ignored.

3.2.4.2 Paper measurement

Knowing the spectra for the major individual components of the newsprint, a prediction of the spectra obtained for a piece of newsprint can be made. It will be a combination of both cellulose and clay spectra, shown in Figure 3.58.

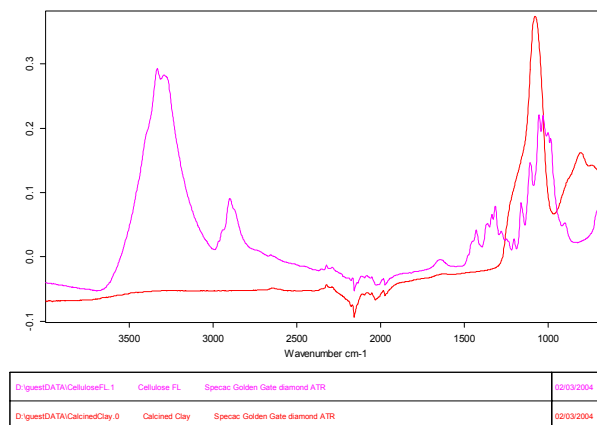


Figure 3.58 – Spectra of Clay and cellulose overlaid.

The cellulose spectra can be subtracted from the spectra of the paper sample to give the filler sample only. The paper sample can then be mapped using reflectance on the FTIR microscope attachment to provide a map of filler distribution across the surface of the paper.

This in turn could be analysed using image analysis software to quantify the particle size distribution of the filler in the paper surface.

FTIR Microspectroscopy equipment is available in APPI, Department of Chemical Engineering, Monash University. The equipment was purchased recently and is currently undergoing commissioning. It was thought that this would be a useful tool to map filler distribution as it has a resolution of 6 μm and the spectra of the fibre and filler should be separable. However this equipment was not available due to problems in commissioning.

This technique has been investigated as a proof of concept and the author recommends that further work be conducted with the FTIR to investigate the method. The infrared beam from the FTIR is focused onto a sample placed in the microscope attachment. The requirements for sample preparation are simple and the sensitivity of detection is high.[28]